



Thank you for using our service!

**Interlibrary Services
The Ohio State University Libraries
(614)292-9077
osuill@osu.edu**

Article Express documents are delivered 24/7 directly to your ILLiad account from scanning libraries around the world. If there is a problem with a PDF you receive, please contact our office so we might report it to the scanning location for resolution.

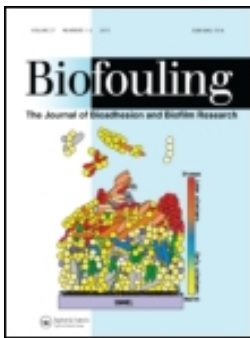
NOTICE

WARNING CONCERNING COPYRIGHT RESTRICTIONS

The copyright law of the United States (Title 17, United States Code) governs the making of photocopies or other reproductions of copyrighted material.

Under certain conditions specified in the law, libraries and archives are authorized to furnish a photocopy or other reproduction. One of these specified conditions is that the photocopy or reproduction is not to be "used for any purpose other than private study, scholarship, or research." If a user makes a request for, or later uses, a photocopy or reproduction for purposes in excess of "fair use," that user may be liable for copyright infringement.

This institution reserves the right to refuse to accept a copying order if, in its judgment, fulfillment of the order would involve violation of copyright law.



Engineered antifouling microtopographies – correlating wettability with cell attachment

Michelle L. Carman , Thomas G. Estes , Adam W. Feinberg , James F. Schumacher , Wade Wilkerson , Leslie H. Wilson , Maureen E. Callow , James A. Callow & Anthony B. Brennan

To cite this article: Michelle L. Carman , Thomas G. Estes , Adam W. Feinberg , James F. Schumacher , Wade Wilkerson , Leslie H. Wilson , Maureen E. Callow , James A. Callow & Anthony B. Brennan (2006) Engineered antifouling microtopographies – correlating wettability with cell attachment, *Biofouling*, 22:1, 11-21, DOI: [10.1080/08927010500484854](https://doi.org/10.1080/08927010500484854)

To link to this article: <http://dx.doi.org/10.1080/08927010500484854>



Published online: 25 Jan 2007.



Submit your article to this journal [↗](#)



Article views: 1051



View related articles [↗](#)



Citing articles: 171 View citing articles [↗](#)

Engineered antifouling microtopographies – correlating wettability with cell attachment

MICHELLE L. CARMAN¹, THOMAS G. ESTES¹, ADAM W. FEINBERG¹,
JAMES F. SCHUMACHER¹, WADE WILKERSON¹, LESLIE H. WILSON²,
MAUREEN E. CALLOW³, JAMES A. CALLOW³ & ANTHONY B. BRENNAN^{1,2}

¹Department of Biomedical Engineering, ²Department of Materials Science and Engineering, University of Florida, Gainesville, FL, USA, and ³School of Biosciences, The University of Birmingham, Birmingham, UK

(Received 28 August 2005; accepted 18 November 2005)

Abstract

Bioadhesion and surface wettability are influenced by microscale topography. In the present study, engineered pillars, ridges and biomimetic topography inspired by the skin of fast moving sharks (Sharklet AFTM) were replicated in polydimethylsiloxane elastomer. Sessile drop contact angle changes on the surfaces correlated well ($R^2 = 0.89$) with Wenzel and Cassie and Baxter's relationships for wettability. Two separate biological responses, i.e. settlement of *Ulva linza* zoospores and alignment of porcine cardiovascular endothelial cells, were inversely proportional to the width (between 5 and 20 μm) of the engineered channels. Zoospore settlement was reduced by $\sim 85\%$ on the finer (*ca* 2 μm) and more complex Sharklet AFTM topographies. The response of both cell types suggests their responses are governed by the same underlying thermodynamic principles as wettability.

Keywords: Biofouling, biomimetic, endothelial, microtopography, wettability, ultrahydrophobic, Ulva

Introduction

Reports on cellular responses to topographical cues on both nanometer and micrometer scales have increased in the past few decades (Singhvi et al. 1994; Curtis & Wilkinson, 1997; Walboomers & Jansen, 2001; Wilkinson et al. 2002). Appropriately scaled nanotopographies have been shown to prevent cell attachment by prohibiting formation of focal contacts (Wilkinson et al. 2002; Arnold et al. 2004). Alternatively, cells can respond to microscale features by altering their shape, such as elongating along grooves (van Kooten & von Recum, 1999; Walboomers & Jansen, 2001). In the area of marine fouling, topography has been shown to deter colonisation of invertebrate shells (Scardino et al. 2003; Bers & Wahl, 2004) and to alter settlement of algae (Callow et al. 2002; Hoipkemeier-Wilson et al. 2004), barnacles (Berntsson et al. 2000) and bacteria (Scheuerman et al. 1998). The change in wettability of a surface that results from surface roughness, i.e. topography, is likely to be a contributing factor to these responses.

Wettability is often characterised in terms of the three-phase contact angle, which relies on the relative interfacial tensions according to Young's equation (Young, 1805):

$$\gamma_{SG} = \gamma_{SL} + \gamma_{LV} \cos \theta \quad (1)$$

Young's equation assumes that the surface is both chemically and topographically homogeneous and does not take into account the dynamic nature of wetting. Many groups have demonstrated the bidirectional nature of surface wetting and therefore, dewetting must be considered also (Johnson & Dettre, 1969; Marmur, 1994; Chen et al. 1999).

Numerous groups have studied the wetting characteristics of topographically rough surfaces. The earliest report that correlates wetting with topography was made by Wenzel (1936), who assumed the contours of the topography become fully wet and the change in contact angle is due to an increase in surface area that topography provides. Wenzel defined a roughness ratio (r) as the surface area divided by the area of the surface when projected

onto a two dimensional plane to account for the change in wetting in terms of contact angle, as follows:

$$\cos \theta^* = r \cos \theta \quad (2)$$

A more detailed approach by Cassie and Baxter (1944) proposed an alternative to the Wenzel equation. They evaluated the wetting by water of waxy surfaces which were not only rough, but also porous. Under this condition, water did not follow the contours of the topography and instead rested upon a composite structure of wax and air. The ratios of the areas of liquid beneath the drop in contact with solid and air relative to the planar surface area were termed f_1 and f_2 respectively. The resulting contact angle (θ_D) for the porous surface was then thermodynamically determined to be the following:

$$\cos \theta_D = f_1 \cos \theta - f_2 \quad (3)$$

More recently, Quéré and colleagues (Bico et al. 1999, 2001, 2002; Quéré, 2002) demonstrated that, for a given surface, regimes of both Wenzel and Cassie-Baxter behaviour exist across a range of liquid surface tensions. They defined the variable ϕ_s as the fraction of liquid beneath the drop in contact with solid. It is equivalent to the f_1 term in Cassie and Baxter's relationship. Air entrapment, fully wetted, and wicking occurs for liquids of sufficiently high, moderate, or low surface tensions, respectively. In the case of wicking, the liquid is drawn into the topography at the advancing edge so that the drop rests on a composite surface of liquid and solid. The corresponding relationships and criteria for each case are given below.

$$\begin{aligned} \text{Air entrapment: } \cos \theta' &= -1 + f_1 (\cos \theta + 1) \\ \text{for } \theta &\geq \cos^{-1} \frac{f_1 - 1}{r - f_1} \end{aligned} \quad (4)$$

$$\begin{aligned} \text{Fully wetted: } \cos \theta' &= r \cos \theta \\ \text{for } \cos^{-1} \frac{1 - f_1}{r - f_1} &\leq \theta \leq \cos^{-1} \frac{f_1 - 1}{r - f_1} \end{aligned} \quad (5)$$

$$\begin{aligned} \text{Wicking: } \cos \theta' &= 1 + f_1 (\cos \theta - 1) \\ \text{for } \theta &\leq \cos^{-1} \frac{1 - f_1}{r - f_1} \end{aligned} \quad (6)$$

Quéré's group also indicated that the air entrapment state would be metastable for the following condition:

$$90^\circ \leq \theta \leq \cos^{-1} \frac{f_1 - 1}{r - f_1} \quad (7)$$

The hypothesis in the present study was that topographic patterns that mimic a natural antifouling surface, viz. the placoid structure of shark skin, may provide a surface with low settlement proper-

ties. A series of engineered microtopographies were replicated in a polydimethylsiloxane elastomer (PDMSe). The engineered patterns included a biomimetic-inspired design based upon the configuration of placoids of fast moving sharks. Changes in wettability were measured and compared against the values predicted by the Wenzel and the Cassie-Baxter relationships. The hypothesis is based upon the assumption that wettability influences the contact-sensing processes of living cells that is part of fouling processes. Two well-characterized but contrasting model systems were used to represent both marine and biomedical fouling, viz. the motile zoospores of the marine alga *Ulva* (syn. *Enteromorpha*), and porcine vascular endothelial cells (PVECs) which form the inner lining of arteries.

The green algal genus *Ulva* (formerly *Enteromorpha*) is the most common macroalga contributing to 'soft' fouling of man-made surfaces throughout the world (Callow, 1986). It is a model system for experimental studies of biofouling and adhesion (Callow et al. 1997; Pettitt et al. 2004; Callow et al. 2005; Chaudhury et al. 2005). Fouling is initiated by the settlement and subsequent adhesion of motile spores, a process which is influenced by a variety of surface-associated cues. Previous laboratory reports show that engineered microtopographies in PDMSe provide specific surface features that promote spore settlement (Callow et al. 2002; Hoipkeimer-Wilson et al. 2004).

Endothelial cells are widely used as models in which to study the influence of substratum morphology on adhesion and contact-mediated growth of animal cells (Riehle et al. 1998; Wilkerson, 2001; Barbucci et al. 2002; Dalby et al. 2002; Gray et al. 2002; Buttiglieri et al. 2003; Magnani et al. 2003). In the present study porcine vascular endothelial cells (PVECs) were chosen because of the local availability of a well-characterised cell line (Zhang et al. 1997). The pig model is an ideal preclinical model for vascular research, as *in vitro* tests have concluded that the coagulation and fibrinolytic systems of swine closely resemble those of humans (Karges et al. 1994; Gross, 1997). In the present study, PVECs are included in the evaluation of the effect of feature spacing (5–20 μm) on cellular orientation. This response is then correlated with the influence of topography on wettability.

Materials and methods

Material

A platinum-catalysed poly(dimethyl siloxane) elastomer (PDMSe) (Dow Corning Corporation's Silastic T-2TM) was used in this study due to its high transparency and reproducibility. The PDMSe

was filled with micron and sub-micron silica particles. In the unmodified state, the polymer is known to promote minimal bioadhesion because of its combination of low surface energy and low modulus (Hoipkemeier-Wilson et al. 2004). The PDMS_e was prepared by mixing ten parts by weight of resin with one part by weight of curing agent. The PDMS_e was typically cured at $\sim 22^\circ\text{C}$ for 24 h.

Pattern designs

The features studied included channels, ridges, pillars, pits and ribs (Figure 1). Channels, ridges, pillars, and pits were $5\ \mu\text{m}$ wide and spaced 5, 10, and $20\ \mu\text{m}$ apart. The rib designs were a reduction of the scales of fast moving sharks. This biologically inspired pattern is referred to as the ‘Sharklet AFTM’, because it is an antifouling topography that was inspired by, but does not match exactly, the skin of the shark. The ribs were $2\ \mu\text{m}$ wide, spaced $2\ \mu\text{m}$ apart, and had lengths ranging from 4– $16\ \mu\text{m}$. Both 1.5 and $5\ \mu\text{m}$ high channel and pillar features were investigated, whereas the ribs of the Sharklet AFTM were $4\ \mu\text{m}$ high.

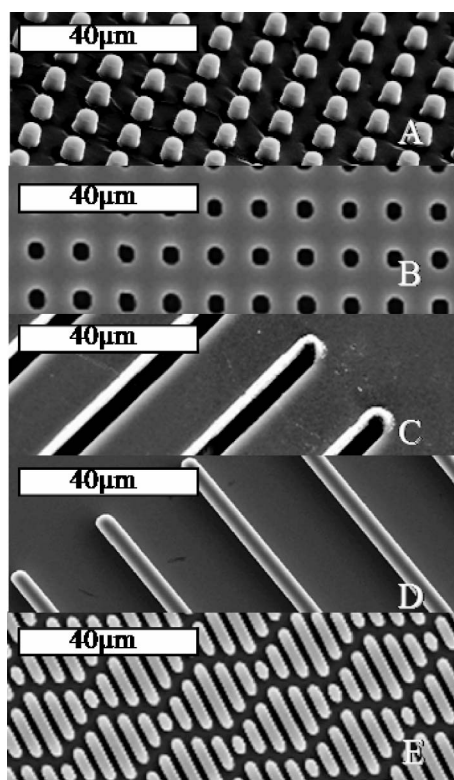


Figure 1. SEM images of PDMS_e microtopographies. Topographies evaluated for wettability and adhesion. A = $5\ \mu\text{m}$ diameter, $5\ \mu\text{m}$ spaced pillars; B = $5\ \mu\text{m}$ diameter, $5\ \mu\text{m}$ spaced pits; C = $5\ \mu\text{m}$ wide, $20\ \mu\text{m}$ spaced channels; D = $5\ \mu\text{m}$ wide, $20\ \mu\text{m}$ spaced ridges; E = Sharklet AFTM topography. Pillars, pits, channels, and were all $5\ \mu\text{m}$ high, while ridges were $1.5\ \mu\text{m}$ high.

Silicon wafer processing

Patterns were etched into silicon wafers using standard photolithography techniques as described previously (Feinberg et al. 2003). Wafers were subsequently critically cleaned using a piranha etch ($50:1\ \text{H}_2\text{SO}_4 / \text{H}_2\text{O}_2$) at 120°C for 10 min followed by subsequent rinsing in acetone and ethanol prior to each replication with PDMS_e. Hexamethyldisilazane was used to methylate the surfaces in order to prevent adhesion.

Pattern transfer and die production

Patterns were transferred to PDMS_e in either negative (channels, pits, and Sharklet AFTM) or positive (pillars and ridges) form (Table I). Negatives were replicated directly from the etched wafer so that the PDMS_e topography was inverted compared to the silicon wafer. For example, pillars in the wafer transfer as pits into the PDMS_e. Positives were generated by first solution casting polystyrene ($0.15\ \text{g ml}^{-1}$ in chloroform) against the wafer followed by curing the PDMS_e against the polystyrene. Epoxy dies (Epon 828 with Jeffamine D230, 9.7:2.73 by weight) were then made from both positively and negatively patterned PDMS_e.

Sample production

Samples in this study included both free-standing PDMS_e films and PDMS_e coatings adhered to glass slides. In both cases, the PDMS_e was cured in a glass

Table I. Dimensions of topographies used in wettability and bioadhesion studies.

Feature	Height (μm)	Width (μm)	Spacing (μm)	Replication type
Pillar	1.5	5	5	Positive
	1.5	5	10	
	1.5	5	20	
	5	5	5	
	5	5	10	
	5	5	20	
Pit	5	5	5	Negative
	5	5	10	
	5	5	20	
Channel	5	5	5	Negative
	5	10	5	
	5	20	5	
Ridge	1.5	5	5	Positive
	1.5	5	10	
	1.5	5	20	
	5	5	5	
	5	5	10	
	5	5	20	
Sharklet AF TM	4	2	2	Negative

mold (Figure 2) as described previously (Callow et al. 2002). Smooth samples were cast directly off the glass, while patterned samples were produced by casting against epoxy or silicon dies. For glass-backed samples, slides were first pretreated with 0.5% allyltrimethoxysilane (ATS) in a 95% ethanol/water solution to improve adhesion. Three replicates of each pattern type were made of each sample topography. The fidelity of the surface features was verified with the aid of light microscopy and SEM.

Contact angle measurements

Wettability was evaluated on free-standing PDMS films containing Sharklet AFTM, 5 μm high channels and pits, and 1.5 μm high ridges by the sessile drop method with 2 μl drops. This method looks at advancing contact angles measured in the first few seconds of contact. Video capture goniometry, coupled with ImageTool software, was used to measure contact angles. Liquids included in the study were nanopure water (17 $\text{M}\Omega\cdot\text{cm}$ resistivity), methylene iodide, and dimethylformamide. Surfaces were rinsed with ethanol and dried at 80°C prior to testing with each liquid. One drop was placed on three replicates of each pattern. Two angle measurements, from the left and right sides of each sample, were taken per drop. In this manner, six measurements were recorded for each pattern. Drops on topographies were viewed from one angle only, which was down the lengths of channels and ribs.

Comparison with model

Wettability data were compared with values predicted by Quéré's combined model of Wenzel and Cassie-Baxter relations. Predicted contacted angles were calculated from the model using the roughness ratios and solid surface fractions of each topography. For both relations, the contact angles on rough

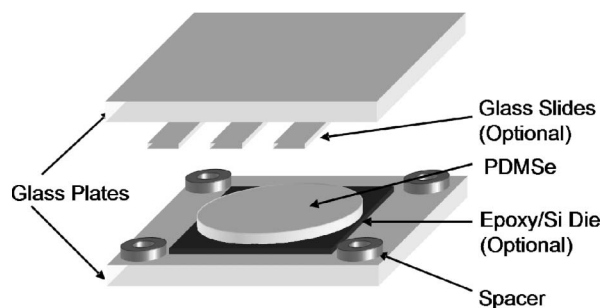


Figure 2. Diagram of the glass mold used to make PDMS samples. The epoxy and silicon dies were used only for patterned samples.

surfaces were related to the contact angle on the smooth surface. In order to account for this, data were normalised by dividing the contact angles for each liquid on textured surfaces by the angle the same liquid makes on smooth PDMS. The normalised values predicted by the models were plotted against normalised values measured on the surfaces. Linear regression was performed to test the statistical validity of the models.

Predicted wetting on novel topographies

Once the model was determined to give a good approximation of the wetting across engineered topographies, it was used to predict the effectiveness of proposed topographies. Topographies considered were circular pillars, square pillars, star-shaped pillars, ring-shaped pillars, a combination of triangular and circular pillars, a gradient array of circular pillars, and hexagonal pillars (Figure 3 and Table II). Both 1 and 3 μm features heights were evaluated. The Sharklet AFTM topography was also considered at these heights to determine effectiveness in altering wettability.

Ulva zoospore assay

PDMS samples containing 5 μm wide ridges and pillars spaced 5, 10 and 20 μm apart at 1.5 and 5 μm heights in addition to the 4 μm high Sharklet AFTM topography were evaluated for settlement of *Ulva* spores. Three replicates of each topography type were tested as films on glass slides. The settlement

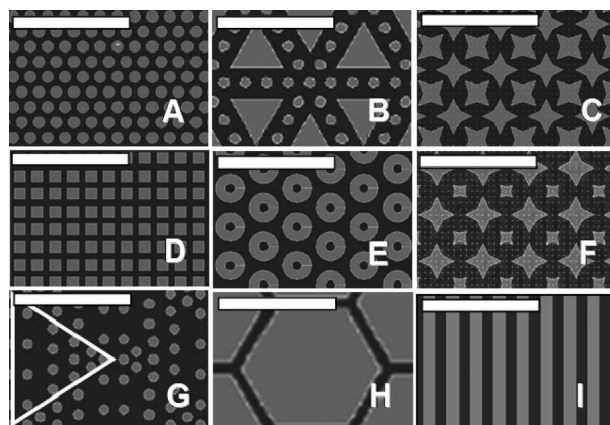


Figure 3. AutoCad sketches of proposed topographies. A = 2 μm diameter, 2 μm spaced pillars; B = triangles and 2 μm pillars; C = 4 μm wide, 2 μm spaced stars; D = 2 μm wide, 1 μm spaced square pillars; E = rings with 2 μm inner diameter and 6 μm outer diameter, spaced 2 μm apart; F = 4 and 2 μm wide stars; G = 2 μm diameter pillars spaced 1, 2 and 4 μm apart in a gradient array (repeat unit designated by triangle); H = hexagons with 12 μm long sides and spaced 2 μm apart; I = 2 μm wide, 2 μm spaced channels. Scale bars = 20 μm .

Table II. Dimensions of novel theoretical topographies.

Feature	Height (μm)	Spacing (μm)	Width (μm)
Circular pillars	1	2	2
	3	2	2
Triangle/Circles	1	2	2,10
	3	2	2,10
Star pillars	1	2	4
	3	2	4
Square pillars	1	1	2
	3	1	2
Ring pillars	1	2	2
	3	2	2
Mixed star pillars	1	2	2,4
	3	2	2,4
Gradient pillars	1	1,2,3,4	2
	3	1,2,3,4	2
Hexagon pillars	1	2	20
	3	2	20
Channels	1	2	2
	3	2	2
Sharklet AF TM	1	2	2
	3	2	2

data for the pillars and ridges were selected from previous publications by the group (Callow et al. 2002; Hoipkemeier-Wilson et al. 2004). The $4\ \mu\text{m}$ Sharklet AFTM topography was evaluated using a similar protocol with one deviation. Samples in this study were shipped to the bioassay site in nanopure water to ensure that air was totally displaced from the features and that the samples remained fully wetted during the assay on the ultrahydrophobic Sharklet AFTM surfaces.

Ulva zoospores were obtained from fertile plants of *Ulva linza* harvested from Wembury Beach, UK ($50^{\circ}18' \text{ N}$; $4^{\circ}02' \text{ W}$) and prepared for experiments as previously described (Callow et al. 1997). Briefly, 10 ml of spore suspension (adjusted to $2 \times 10^6 \text{ ml}^{-1}$) were added to each sample and incubation was carried out for 60 min in the dark followed by fixation with 2% glutaraldehyde in artificial seawater (Instant OceanTM). Settled spore counts were taken using a $\times 10$ objective with a Zeiss Kontron 3000 image analysis system attached to a Zeiss epifluorescence microscope and video camera as described by Callow et al. (2002). Thirty images of each of the three replicate samples were photographed to quantify the number of attached spores. Photographic images were taken at 1 mm intervals along the axis of the slide of both smooth and textured areas of the patterned slides. Spore settlement data are reported as the mean number of adhered spores ($x=90$) with 95% confidence limits.

Porcine vascular endothelial cell (PVEC) assay

PVEC cell attachment was evaluated on free-standing PDMSe samples containing 5, 10, and $20\ \mu\text{m}$ spaced, $5\ \mu\text{m}$ wide ridges at both 1.5 and $5\ \mu\text{m}$ heights. PDMSe was coated with fibronectin (FN) using the method of Ostuni and Whitesides (Ostuni et al. 2001) to promote cell attachment by conversion from hydrophobic to a hydrophilic surface. Briefly, lyophilised bovine plasma FN (Sigma) was dissolved in 2 ml of $0.22\ \mu\text{m}$ filtered water at 37°C for 45 min and diluted to $50\ \mu\text{g ml}^{-1}$ in Hanks Balanced Salt Solution (HBSS). Sterilised samples were placed in individual wells of a 24-well plate, and FN was added in 0.5 ml aliquots to each sample. During exposure to vacuum (100 kPa) to remove trapped air (which could cause denaturation of the FN, which could affect initial cell adhesion (Ward et al. 1979)), samples were left to incubate for 1 h at room temperature. The FN solution was aspirated out and then the samples were washed three times with HBSS.

PVECs obtained from the main pulmonary artery of 6 to 7-month-old pigs were supplied by Dr Edward Block's lab between passages 2 and 5 (Patel et al. 1988). Cells were seeded at a density of 2×10^5 cells per sample in 1 ml of serum-free medium. Serum-free medium was selected because an adhesion protein (FN) was already adsorbed on sample surfaces. The cells were incubated at 37°C and 5% CO_2 for 48 to 72 h.

Samples were fixed with cold 10% n-buffered formalin for 20 min. The cell bodies were then stained for 20 min in 1% crystal violet solution. Hematoxylin (Richard Allan Scientific) was used to stain cell nuclei so that nuclear elongation could be used to quantify contact guidance. Cells were stained in hematoxylin for 2 min.

Cells were imaged on the surface at $200\times$ magnification using a Nikon Optiphot microscope and Matrox image capturing system. Multiple images were taken at each feature width that included at least 5 nuclei. A nuclear form factor (NFF) was determined for each cell by calculating the log of the ratio of cell nucleus length to width at its widest point (Figure 4) (Dunn & Heath, 1976). A 5×5 grid was superimposed on the images, and 5 nuclei were chosen per image, each from a separate square of the grid. Using this method, at least 20 nuclei per topography type were quantified.

Statistical methods

Results are reported using mean values and 95% confidence intervals. One-way analysis of variance (ANOVA) and multiple comparison tests (Tukey, 95% confidence interval) were used to compare groups.

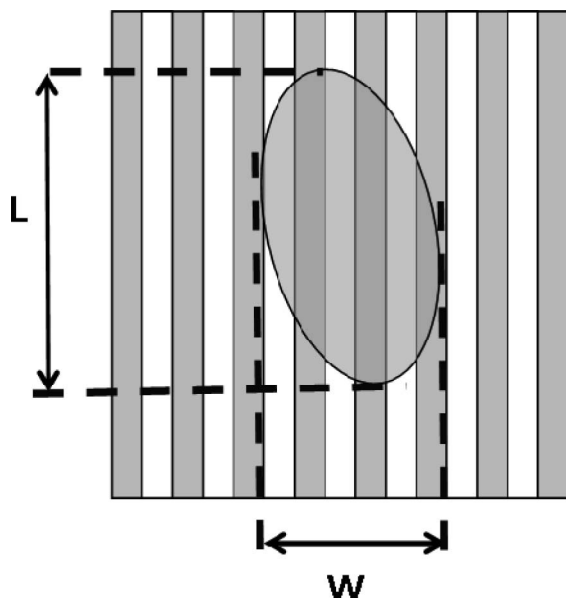


Figure 4. Schematic of the measurements taken to calculate nuclear form factor where L is the length of the nucleus parallel to the ridges and W is the width of the nucleus orthogonal to the ridges.

Results

Contact angle measurements

As expected, topography increased water contact angles and decreased both methylene iodide and dimethyl formamide contact angles (Table III). The most effective topography at altering wettability was the Sharklet AFTM, whereas the 20 μm spaced ridges and pits behaved most like smooth PDMS. The water contact angle on PDMS increased by 20%, while the contact angles of methylene iodide and dimethyl formamide reduced by 35% and 33%, respectively. Droplets on the pits and Sharklet AFTM maintained a circular contact area, whereas droplets on the channels and ridges elongated along the features. Because of their cylindrical, rather than spherical, geometry the contact angles on the channels and ridges are treated as estimates.

Receding contact angles were not evaluated by the captive air method because of difficulty in bubble placement. For example, the channel patterns were only 0.33 cm wide (Figure 5) and the topographies became invisible upon wetting. Consequently, it was not possible to be certain that the air bubble remained in the desired region. In addition, the Wilhelmy plate technique was also deemed unsuitable because of the inability to prepare a proper sample (same topography on all sides).

The effect of topography height was examined by comparing the 5 μm spaced, 5 μm high channels against the 5 μm spaced and 1.5 μm high ridges. Because droplets were placed away from the pattern boundaries, the feature height was the only difference

Table III. Measured contact angles on microtopographies.

Features	Spacing (μm)	f_1	R	Contact Angles ($^\circ$)		
				Water	MeI	DMF
Smooth	–	1.00	1.0	108 \pm 4	71 \pm 6	55 \pm 8
Pits	5	0.80	1.8	115 \pm 2	65 \pm 2	50 \pm 8
	10	0.91	1.4	112 \pm 2	69 \pm 4	52 \pm 4
	20	0.97	1.1	110 \pm 6	65 \pm 6	56 \pm 6
Channels	5	0.50	2.0	133 \pm 8	51 \pm 2	39 \pm 6
	10	0.67	1.7	121 \pm 6	62 \pm 4	49 \pm 8
	20	0.80	1.4	116 \pm 6	68 \pm 12	48 \pm 6
Ridges	5	0.50	1.3	116 \pm 8	63 \pm 8	46 \pm 4
	10	0.33	1.2	115 \pm 8	63 \pm 6	46 \pm 8
	20	0.20	1.1	111 \pm 6	66 \pm 4	52 \pm 8
Sharklet AF TM	2	0.47	4.2	135 \pm 3*	46 \pm 8	35 \pm 2

*Indicates droplet would not settle on the surface and had to be captured with video.

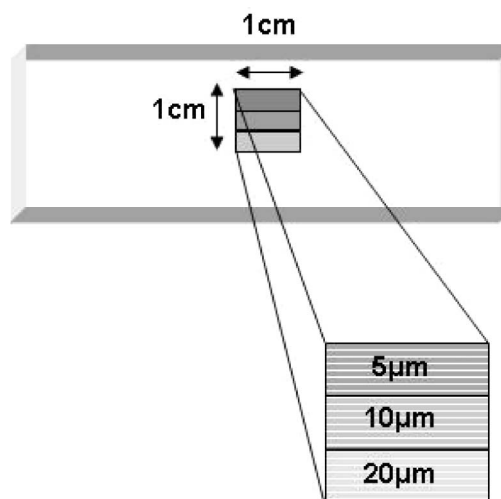


Figure 5. Layout of channel topographies. Each channel width (5, 10 and 20 μm) was contained within a 1 cm \times 0.33 cm area.

sensed by the spreading drops. The water contact angle was significantly greater on the 5 μm high channel compared to the 1.5 μm high ridge. The effect of feature spacing was examined by looking at trends within the pits, channels, and ridge topographies. Increased feature spacing and decreased pattern depth resulted in diminished contact angle changes.

Comparison with model

The sessile drop contact angle data were compared against the model to determine their viability for use in prescreening new patterns. The 1.5 μm high ridges have relatively low roughness factors (1.1–1.3) and solid fractions (0.2–0.5). On these surfaces, water droplets appeared to follow the situation proposed by Wenzel (Figure 6) rather than the metastable state

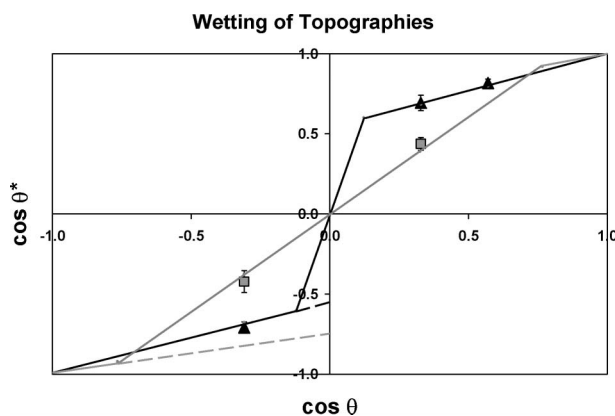


Figure 6. Change in wettability induced by the 20 μm spaced ridges (\square) and Sharklet AFTM (\blacktriangle) topographies compared to smooth PDMS_e. Both measured data and model predictions are given. ---- = the metastable air pocket state proposed by Quéré.

described by Quéré. The Sharklet AFTM topography, on the other hand, has a high roughness factor (4.2) and moderate solid fraction (0.47), and all three test liquids exhibited the behaviour described by Cassie (air pockets or wicking).

Quéré proposed that air entrapment would be favoured for liquids of sufficiently high surface tensions ($\theta > \cos^{-1}[(f_i - 1)/(r - f_i)]$) and would be metastable for liquids satisfying the condition of $90^\circ < \theta < \cos^{-1}[(f_i - 1)/(r - f_i)]$. The results in Figure 6, however, suggest that the metastable air pocket state is not favoured and that, instead, the Wenzel regime is followed. Consequently, the model was adapted to eliminate the metastable state. In order to test the reliability of the adapted model, data were normalised with respect to the smooth contact angles. The model fits the data well ($y = 0.99x$) with a coefficient of determination of 0.89 (Figure 7).

Predicted wettability on novel topographies

The model predicts that the hexagons would be the least effective at increasing the hydrophobic nature of PDMS_e (Table IV) relative to the various designs, i.e. circular pillars, square pillars, star-shaped pillars, combination of triangular and circular pillars, and gradient array of circular pillars. The results reveal a minimal increase of only 1° and 3° in the water contact angle for the 1 and 3 μm high hexagonal features in PDMS_e, respectively. These changes are insignificant when considered against the typical standard error in contact angle measurements of 3° . The model predicts that the 3 μm high mixed star pattern would be the most effective and lead to an increase in water contact angle of approximately 31° relative to smooth PDMS_e. A maximum height of 3 μm was chosen for this investigation because 2 μm diameter pillars in PDMS_e tended to collapse at higher aspect ratios (Figure 8).

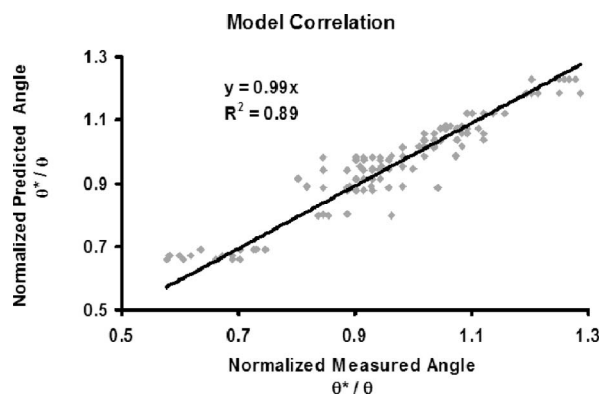


Figure 7. Graph comparing contact angles predicted by the model with contact angles measured on the surfaces. Data were normalised with respect to contact angles on smooth PDMS_e. Linear regression indicates a near 1:1 relationship (slope=0.99) with high correlation ($R^2 = 0.89$) to the data.

All pattern types were predicted to be fully wetted by water when feature heights were held to 1 μm . Increasing the height to 3 μm , however, should promote the trapping of air in all topographies except the hexagons, circular pillars, and gradient pillars.

Ulva zoospore assay

The ridge topographies enhanced spore settlement (Figure 9). The most significant effect was observed on the 5 μm spaced, 5 μm high ridges, which increased settlement by 150% relative to the smooth surface. This dimension is roughly equivalent to the diameter of the pear-shaped swimming spore at its widest point and the diameter of the settled spore (Figure 10). As spacing increased, the density of settled spores approached that of smooth PDMS_e. Settlement density decreased on the shorter 1.5 μm high ridges in comparison to the 5 μm high ridges, but still remained at least as great as the density on smooth PDMS_e. Settlement was limited almost entirely to valley regions for all ridge topographies.

The Sharklet AFTM topography, which had feature dimensions smaller than the spore body, significantly reduced settlement density by $\sim 86\%$ relative to smooth PDMS_e (Figure 9). Spores avoided the 2 μm wide channels and were largely confined to defects and slightly wider spaces ($\sim 3 \mu\text{m}$) located between adjacent Sharklet AFTM diamonds (Figure 10).

PVEC assay

PVEC growth on smooth PDMS_e was random with respect to orientation. Consequently, NFFs were essentially zero (Figure 11). Cells attached to ridge pattern substrata became aligned with the topographies. The PVECs settled almost entirely in the valleys formed by adjacent ridges similar to the *Ulva* spores (Figure 12). Cell orientation was most

Table IV. Predicted water contact angles on theoretical topographies.

Feature	Height (μm)	Spacing (μm)	Width (μm)	r	F ₁	θ^*	Wetting regime
Circular pillars	1	2	2	1.39	0.06	118	Wenzel
	3	2	2	2.18	0.06	138	Wenzel
Triangle/Circles	1	2	2,10	1.65	0.49	121	Wenzel
	3	2	2,10	2.94	0.49	132	C&B
Star pillars	1	2	4	1.7	0.57	122	Wenzel
	3	2	4	3.09	0.57	127	C&B
Square pillars	1	1	2	1.89	0.44	128	Wenzel
	3	1	2	3.67	0.44	134	C&B
Ring pillars	1	2	2	1.45	0.45	117	Wenzel
	3	2	2	2.36	0.45	133	C&B
Mixed star pillars	1	2	2,4	1.52	0.36	118	Wenzel
	3	2	2,4	2.57	0.36	139	C&B
Gradient pillars	1	1,2,3,4	2	1.35	0.18	115	Wenzel
	3	1,2,3,4	2	2.06	0.18	130	Wenzel
Hexagon pillars	1	2	20	1.06	0.91	109	Wenzel
	3	2	20	1.17	0.91	111	Wenzel
Channels	1	2	2	1.5	0.5	119	Wenzel
	3	2	2	2.5	0.5	132	C&B
Sharklet AF TM	1	2	2	1.79	0.47	124	Wenzel
	3	2	2	3.38	0.47	132	C&B

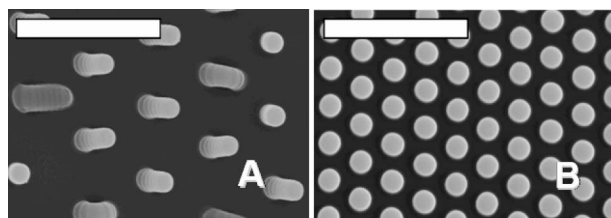


Figure 8. SEM images of $2\ \mu\text{m}$ diameter pillars in PDMS. A = $5\ \mu\text{m}$ high and $4\ \mu\text{m}$ spaced; B = $3\ \mu\text{m}$ high and $2\ \mu\text{m}$ spaced. Increased height caused pillars to bend. Scale bars = $15\ \mu\text{m}$.

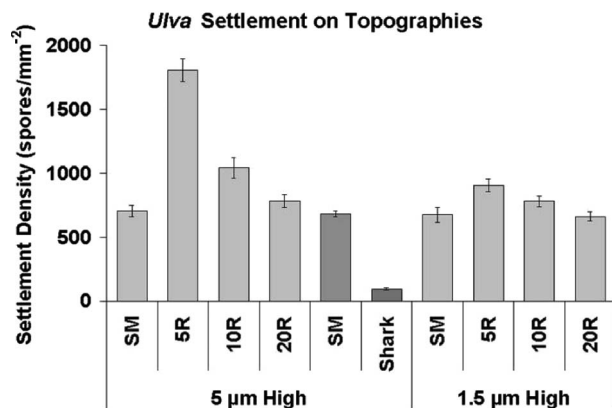


Figure 9. *Ulva* settlement on smooth (SM) and textured PDMS. Topographies studied included the Sharklet AFTM (Shark) in addition to $5\ \mu\text{m}$ wide ridges that were 5, 10, and $20\ \mu\text{m}$ spaced, (5R, 10R, and 20R) and 1.5 or $5\ \mu\text{m}$ high. The Sharklet AFTM topography was evaluated in a separate experiment as indicated by the darker bars. Error bars = ± 2 SEs of the mean. For all surfaces, counts are based on the mean of 90 counts, 30 from each of 3 replicates.

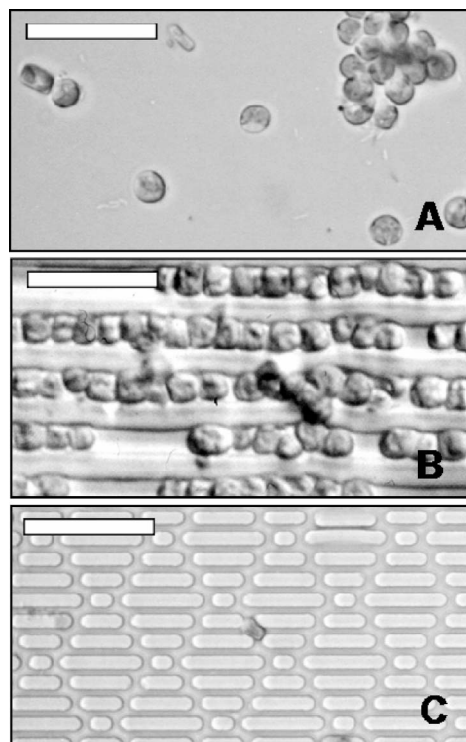


Figure 10. Images of *Ulva* settlement on (A) a smooth surface; (B) $5\ \mu\text{m}$ wide, $5\ \mu\text{m}$ spaced, and $5\ \mu\text{m}$ high channels and (C) $4\ \mu\text{m}$ high Sharklet AFTM in PDMS. Images were taken via light microscopy. Scale bars = $25\ \mu\text{m}$.

strongly directed by the $5\ \mu\text{m}$ high, $5\ \mu\text{m}$ spaced ridges. NFFs varied directly with feature height and inversely with feature spacing for $5\ \mu\text{m}$ high features (Figure 11).

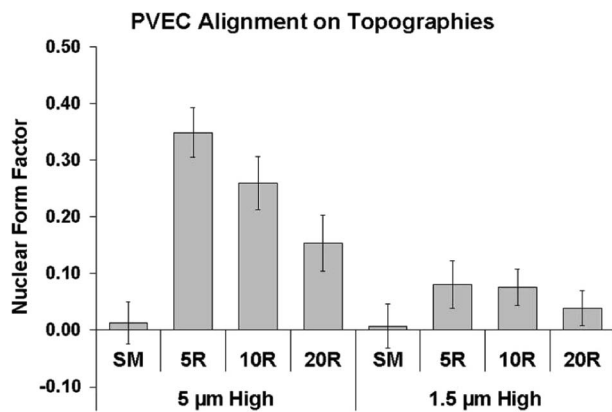


Figure 11. PVEC alignment on smooth (SM) and textured PDMS. Topographies studied were 5, 10, and 20 μ m spaced, 5 μ m wide ridges (5R, 10R, and 20R) that were both 1.5 and 5 μ m high. Error bars = ± 2 SEs of the mean.

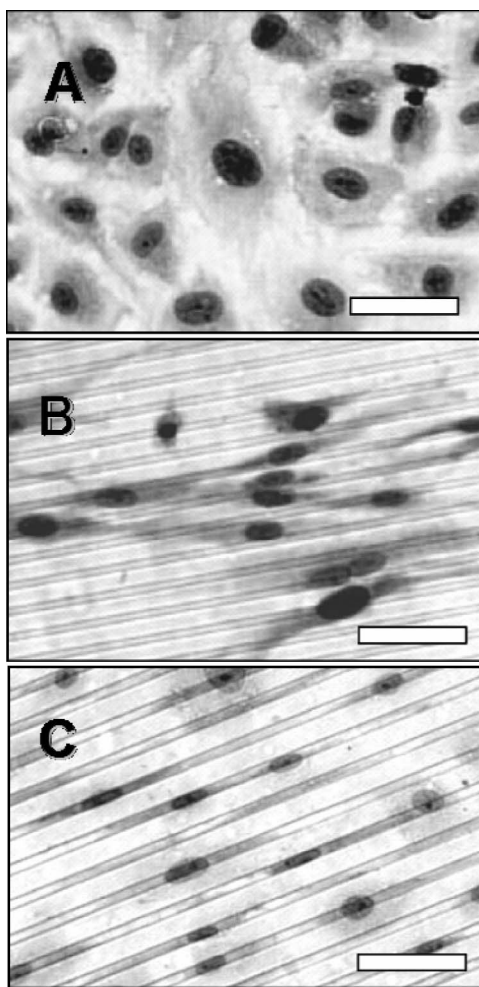


Figure 12. Endothelial cells grown on (A) a smooth surface, (B) 5 μ m wide, 5 μ m spaced, and 5 μ m high ridges, and (C) 5 μ m wide, 5 μ m spaced, and 1.5 μ m high ridges. Images have been processed to improve contrast. Scale bars = 50 μ m.

The NFFs were significantly different for all widths at the 5 μ m depth. NFFs differed significantly only for cells on channels at the 1.5 μ m height with

the 5 μ m wide ridges. One of the difficulties in the analysis is the fact that the nuclei were not round, but rather elongated in random directions on the smooth FN-treated PDMS samples. Consequently, the mean nuclear form factors for smooth areas were near zero, but with a large standard deviation.

Discussion

Researchers report independently that topography alters wettability (Wenzel, 1936; Cassie & Baxter, 1944) and surface energy influences bioadhesion (Dexter, 1976; Kaelble & Moacanin, 1977; Baier, 1982; Baier et al. 1984; Finlay et al. 2002). This study investigates the interrelationship of all three factors (topography, wettability and adhesion) simultaneously using two different cell types viz. motile algal spores, which ‘choose’ where to settle and adhere, and cultured animal cells (PVEC), which are known to adapt to underlying substratum morphology. The wetting response is well-described by the Wenzel and Cassie-Baxter equations for the topographies investigated, but ideally it would be desirable also to predict the effect of topography on bioadhesion. It is interesting to note that both biological models responded to the channel topographies by attempting to fill the valleys either through packing of settled cells (*Ulva*) or by cell elongation (PVECs). This suggests that their responses are governed by the same underlying thermodynamic principles as wettability. Consider a cell settling on a textured surface. If the cell is too large to rest between or on top of the features, it must bridge, align, or conform to their shape. Bridging is similar to the air pocket state and alignment is similar to the wicking states described by the Cassie-Baxter relation. Alternatively, conforming resembles Wenzel behaviour.

Consider a surface that an organism will settle on, but for which it has a relatively low affinity (e.g. PDMS for *Ulva* spores). If the topography of this surface is engineered to expand the Cassie-Baxter regime, then the organism may be induced to bridge the features. **Bridging will increase tension along the unsupported regions of the organism’s membrane. Additionally, bridging would be expected to reduce the area of contact between the organism and surface, which would reduce the overall adhesion strength.** Thus, bridging reduces the potential for settlement by creating unfavourable energy barriers. This would be very useful, particularly in limiting marine fouling.

Using this hypothesis, the Sharklet AFTM topography was engineered to enhance hydrophobicity with dimensions smaller than the *Ulva* spore so that bridging is necessary for settlement. It is important to note that the Sharklet AFTM design is biomimetically inspired rather than a true biomimic. Although the

basic pattern of the placoids is maintained, the dimensions are reduced and the tips of the ribs are flattened. As designed, spores avoided the topography which reduced settlement density by 86%. This result provides the first demonstration of an engineered microtopography inhibiting the settlement of spores of a marine alga.

In addition to preventing settlement, topographies also can be engineered to promote it. Consider an organism settling on a surface which it prefers (e.g. PVECs on fibronectin-coated PDMSe). If the topography of this surface is engineered to expand the Cassie regime, then the organism may be induced to align with the topographic features. This is evident in the PVEC study presented here. For the topographies studied, the Cassie-Baxter regime increased with increased spacing and increased depth. Similarly, PVEC alignment, i.e. NFFs, increased in response to increased spacing and depth of the channels. This is consistent with research by the von Recum group demonstrating that rat dermal fibroblasts become increasingly oriented on 0.5 μm high microgrooves as the width is reduced from 10 to 2 μm (Schmidt & von Recum, 1991; den Braber et al. 1996, 1998; van Kooten & von Recum, 1999).

Microbubbles on surfaces are reported to denature surface adsorbed proteins, which increases cell adhesion (Ward et al. 1979). Fibronectin pretreatment of PDMSe was used in the PVEC assay to convert the surface to a hydrophilic surface needed for initial cell attachment. To minimise any potential artefacts in the PVEC assay that could be caused by differential fibronectin adsorption through the presence of microbubbles, all PDMSe surfaces were degassed during fibronectin adsorption to eliminate surface-adsorbed air bubbles from topographies. It can therefore be concluded that it is unlikely that the results on PVEC alignment can be ascribed to artefacts caused by microbubbles. In the case of *Ulva* spore settlement, it can also be reported that hydrophilic modification of the topographies (which would eliminate microbubble formation) did not alter the inhibition of zoospore settlement by the sharklet topography (Wilson et al. 2005). Thus, it is concluded that *Ulva* zoospores were contact sensing the topography and were not influenced by the presence of microbubbles.

These results demonstrate the importance of wettability models in predicting cellular contact guidance for engineered topographies, but do not fully explain the process. Bioadhesion is a complex and species-specific process (Qian et al. 2000). The material modulus and surface elasticity of the cell membrane are other factors to consider, in addition to the variety of adhesive proteins, glycoproteins, and polysaccharides that organisms secrete. Wettability models are

limited by the assumption that the liquid droplet is much larger than the topographical features. This allows for line tension effects to be neglected. Measurements with smaller drop sizes are believed to enable the inclusion of line tension effects. Ultimately, the goal is to improve the predictive quality of an energy-driven model for predicting bioadhesion.

Acknowledgements

ABB gratefully acknowledges the financial support of the Office of Naval Research (Contract No. N00014-02-1-0325) and the National Institutes of Health (Contract No. R01 DE 13492-01) to fund this research. JAC and MEC acknowledge financial support from the Office of Naval Research (Award N00014-02-05121). Porcine vascular endothelial cells were graciously donated by Dr Edward Block, Malcom Randall Veteran's Administration Hospital, Gainesville, FL.

References

- Arnold M, Cavalcanti-Adam EA, Glass P, Blummel J, Eck W, Kantelechner M, Kessler H, Spatz JP. 2004. Activation of integrin function by nanopatterned adhesive interfaces. *Chem Phys Chem* 5:383–388.
- Baier RE. 1982. On adhesion of biological substances to low energy solid surfaces. *J Colloid Interface Sci* 88:296–297.
- Baier RE, Meyer AE, Natiella JR, Natiella RR, Carter JM. 1984. Surface properties determine bioadhesive outcomes: methods and results. *J Biomed Mater Res* 18:337–355.
- Barbucci R, Lamponi S, Magnani A, Pasqui D. 2002. Micro-patterned surfaces for the control of endothelial cell behaviour. *Biomol Eng* 19:161–170.
- Berntsson KM, Jonsson PR, Lejhall M, Gatenholm P. 2000. Analysis of behavioural rejection of micro-textured surfaces and implications for recruitment by the barnacle *Balanus improvisus*. *J Exp Mar Biol Ecol* 251:59–83.
- Bers AV, Wahl M. 2004. The influence of natural surface microtopographies on fouling. *Biofouling* 20:43–51.
- Bico J, Marzolin C, Quéré D. 1999. Pearl drops. *Europhys Lett* 47:220–226.
- Bico J, Tordeux C, Quéré D. 2001. Rough wetting. *Europhys Lett* 55:214–220.
- Bico J, Thiele U, Quéré D. 2002. Wetting of textured surfaces. *Colloids Surf A: Physicochem Eng Aspects* 206:41–46.
- Buttiglieri S, Pasqui D, Migliori M, Johnstone H, Affrossman S, Sereni L, Wratten ML, Barbucci R, Tetta C, Camussi G. 2003. Endothelialization and adherence of leucocytes to nanostructured surfaces. *Biomaterials* 24:2731–2738.
- Callow JA, Callow ME, Ista LK, Lopez G, Chaudhury MK. 2005. The influence of surface energy on the wetting behaviour of the spore adhesive of the marine alga *Ulva linza* (syn. *Enteromorpha linza*). *J R Soc Interface* 2:319–325.
- Callow ME. 1986. Fouling algae from 'in-service' ships. *Bot Mar* 24:351–357.
- Callow ME, Callow JA, Pickett-Heaps J, Wetherbee R. 1997. Primary adhesion of *Enteromorpha* (*Chlorophyta*, *Ulvales*) propagules: quantitative settlement studies and video microscopy. *J Phycol* 33:938–947.

- Callow ME, Jennings AR, Brennan AB, Seegert CA, Wilson L, Feinberg A, Baney R, Callow JA. 2002. Microtopographic cues for settlement of zoospores of the green fouling alga *Enteromorpha*. *Biofouling* 18:237–245.
- Cassie ABD, Baxter S. 1944. Wettability of porous surfaces. *Faraday Soc Trans* 40:546–551.
- Chaudhury MK, Finlay JA, Chung JY, Callow ME, Callow JA. 2005. The influence of elastic modulus on the soft fouling alga *Ulva linza* (*Enteromorpha linza*) from polydimethyl siloxane (PDMS) ideal networks. *Biofouling* 21:41–48.
- Chen W, Fadeev AY, Hsieh MC, Oner D, Youngblood J, McCarthy TJ. 1999. Ultrahydrophobic and ultrahydrophilic surfaces: some comments and examples. *Langmuir* 15:3395–3399.
- Curtis A, Wilkinson C. 1997. Review: topographical control of cells. *Biomaterials* 18:1573–1583.
- Dalby MJ, Riehle MO, Johnstone H, Affrossman S, Curtis ASG. 2002. *In vitro* reaction of endothelial cells to polymer demixed nanotopography. *Biomaterials* 23:2945–2954.
- den Braber ET, de Ruijter JE, Ginsel LA, von Recum AF, Jansen JA. 1998. Orientation of ECM protein deposition, fibroblast cytoskeleton, and attachment complex components on silicone microgrooved surfaces. *J Biomed Mater Res* 40:291–300.
- den Braber ET, de Ruijter JE, Smits HTJ, Ginsel LA, von Recum AF, Jansen JA. 1996. Quantitative analysis of cell proliferation and orientation on substrata with uniform parallel surface micro-grooves. *Biomaterials* 17:1093–1099.
- Dexter SC. 1976. Influence of substrate wettability on the formation of bacterial slime films on solid surfaces immersed in natural sea water. *Int Congr Mar Corrosion Fouling* 4:137–144.
- Dunn GA, Heath JP. 1976. A new hypothesis of contact guidance in tissue cells. *Exp Cell Res* 101:1–14.
- Feinberg AW, Gibson AL, Wilkerson WR, Seegert CA, Wilson LH, Zhao LC, Baney RH, Callow JA, Callow ME, Brennan AB. 2003. Investigating the energetics of bioadhesion on microengineered siloxane elastomers: characterizing the topography, mechanical properties, and surface energy and their effect on cell contact guidance. In: Clarson SJ, Fitzgerald JJ, Owen MJ, Smith SD, van Dyke ME, editors. *Synthesis and properties of silicones and silicone-modified materials*. *Am Chem Soc* 838:196–211.
- Finlay JA, Callow ME, Ista LK, Lopez GP, Callow JA. 2002. The influence of surface wettability on the adhesion strength of settled spores of the green alga *Enteromorpha* and the diatom *Amphora*. *Integr Comp Biol* 42:1116–1122.
- Gray BL, Lieu DK, Collins SD, Smith RL, Barakat IL. 2002. Microchannel platform for the study of endothelial cell shape and function. *Biomed Microdevices* 4:9–16.
- Gross DR. 1997. Thromboembolic phenomena and the use of the pig as an appropriate animal for research on cardiovascular devices. *Int J Artif Org* 20:195–203.
- Hoipkemeier-Wilson L, Schumacher JF, Carman ML, Gibson AL, Feinberg AW, Callow ME, Finlay JA, Brennan AB. 2004. Antifouling potential of lubricious, micro-engineered, PDMS elastomers against zoospores of the green fouling alga *Ulva*. *Biofouling* 20:53–63.
- Johnson RE Jr, Dettre RH. 1969. Wettability and contact angles. *Surf Coll Sci* 2:85–153.
- Kaelble DH, Moacanin J. 1977. A surface energy analysis of bioadhesion. *Polymer* 18:475–482.
- Karges HE, Funk KA, Ronneberger H. 1994. Activity of coagulation and fibrinolysis parameters in animals. *Arzneimittelforschung/Drug Res* 44:793–797.
- Magnani A, Priamo A, Pasqui D, Barbucci R. 2003. Cell behaviour on chemically microstructured surfaces. *Mater Sci Eng C* 23:315–328.
- Marmur A. 1994. Thermodynamic aspects of contact angle hysteresis. *Adv Colloid Interface Sci* 50:121–141.
- Ostuni E, Chen CS, Ingber DE, Whitesides GM. 2001. Selective deposition of proteins and cells in arrays of microwells. *Langmuir* 17:2828–2834.
- Patel JM, Edwards DA, Block ER, Raizada MK. 1988. Effect of nitrogen-dioxide on surface-membrane fluidity and insulin-receptor binding of pulmonary endothelial-cells. *Biochem Pharmacol* 37:1497–1507.
- Pettitt ME, Henry SL, Callow ME, Callow JA, Clare AS. 2004. Activity of commercial enzymes on the settlement and adhesion of cypris larvae of the barnacle *Balanus amphitrite*, spores of the green alga *Ulva linza* and the diatom *Navicula perminuta*. *Biofouling* 20:299–311.
- Qian P-Y, Rittschof D, Sreedhar B. 2000. Macrofouling in unidirectional flow: miniature pipes as experimental models for studying the interaction of flow and surface characteristics on the attachment of barnacle, bryozoan and polychaete larvae. *Mar Ecol Prog Ser* 207:109–121.
- Quérel D. 2002. Rough ideas on wetting. *Physica A: Stat Theoret Phys* 313:32–46.
- Riehle M, Ferris D, Hamilton D, Curtis A. 1998. Cell behavior in tubes. *Exp Biol Online* 3(2).
- Scardino A, De Nys R, Ison O, O'Connor W, Steinberg P. 2003. Microtopography and antifouling properties of the shell surface of the bivalve molluscs *Mytilus galloprovincialis* and *Pinctada imbricata*. *Biofouling* 19:221–230.
- Scheuerman TR, Camper AK, Hamilton MA. 1998. Effects of substratum topography on bacterial adhesion. *J Colloid Interface Sci* 208:23–33.
- Schmidt JA, von Recum AF. 1991. Texturing of polymer surfaces at the cellular level. *Biomaterials* 12:385–389.
- Singhvi R, Stephanopoulos G, Wang DIC. 1994. Review: effects of substratum morphology on cell physiology. *Biotechnol Bioeng* 43:764–771.
- van Kooten TG, von Recum AF. 1999. Cell adhesion to textured silicone surfaces: the influence of time of adhesion and texture on focal contact and fibronectin formation. *Tiss Eng* 5:223–240.
- Walboomers XF, Jansen JA. 2001. Cell and tissue behavior on micro-grooved surfaces. *Odontology* 89:2–11.
- Ward CA, Stanga D, Zdasink BJ, Gates FL. 1979. Effect of air nuclei on the adsorption of fibrinogen to silicone rubber. *Ann Biomed Eng* 7:451–469.
- Wenzel RN. 1936. Resistance of solid surfaces to wetting by water. *Ind Eng Chem* 28:988–994.
- Wilkerson WR. 2001. Contribution of modulus to the contact guidance of endothelial cells on microtextured siloxane elastomers. University of Florida: Gainesville, FL. 97.
- Wilkinson CDW, Riehle M, Wood M, Gallagher J, Curtis ASG. 2002. The use of materials patterned on a nano- and micro-metric scale in cellular engineering. *Mater Sci Eng C* 19:263–269.
- Wilson LH, Schumacher JF, Finlay JA, Perry R, Callow ME, Callow JA, Brennan AB. 2005. Towards minimally fouling substrates: surface grafting and topography. *Polymer Preprints* 46:1312–1313.
- Young T. 1805. An essay on the cohesion of fluids. *Philos Trans R Soc Lond* 95:65–87.
- Zhang J, Patel JM, Block ER. 1997. Molecular cloning, characterization and expression of a nitric oxide synthase from porcine pulmonary artery endothelial cells. *Comp Biochem Physiol B: Biochem Molec Biol* 116:485–491.

